


Initialization, manipulation, and readout of chiral qubits by bias and inhomogeneous Zeeman field in triangular triple quantum dots

Yue Qi¹, Wen-Jie Hou², Yuan-dong Wang^{3,*} and Jian-Hua Wei^{1,†}

¹*Department of Physics, Renmin University, Beijing 100876, China*

²*Institute of Fundamental and Frontier Sciences, University of Electronic Science and Technology of China, Chengdu 610054, China*

³*School of Electronic, Electrical and Communication Engineering, University of Chinese Academy of Sciences, Beijing 100049, China*

 (Received 29 December 2023; revised 21 March 2024; accepted 19 April 2024; published 3 June 2024)

We realize the initialization, manipulation, and readout of qubits in triangular triple quantum dots (TTQDs) with theoretical and numerical simulation calculations. In the initialization, the degenerate ground states can be split by adding a vertical magnetic flux or a bias voltage at the initial time. This is consistent with the magnetoelectric equivalence proposed in previous work, and both cause chiral state splitting. In the manipulation, we add an inhomogeneous Zeeman field to the TTQDs. Based on the Heisenberg model of the two-level system, it is obtained that the applied Zeeman field gradient will cause Rabi oscillation of the two chiral states' occupation probability, which also corresponds to the manipulation of chiral qubits on the Bloch sphere. The Rabi cycle and amplitude vary with the gradient of the Zeeman field and the internal chiral term, and numerical simulation is consistent with the theoretical results. Finally, we give a possible readout method to use for the topological blockage of chiral and conduction current. This method provides an alternative idea for qubits, which can realize quantum coding by using the smallest chiral topological structure.

DOI: [10.1103/PhysRevB.109.245105](https://doi.org/10.1103/PhysRevB.109.245105)

I. INTRODUCTION

Quantum computing is the inevitable product of semiconductor chip size breaking through the classical physical limits. Encoding qubits using the quantum properties of electrons in semiconductor quantum dots (QDs) is one of the most likely candidates to achieve quantum computing [1–6]. In the QD system, two quantum states can be easily obtained to characterize the basic unit of quantum information, qubits, and the target state of the system can be easily prepared. During the manipulation of qubits, the QD system can also perform arbitrary operations on a single qubit, thus implementing controlled nongate operations [7–12].

Many investigations have discovered that any two-level quantum system can be used as a qubit. The aim of quantum information processing is to control and manipulate the dynamic behavior of qubit system to make it evolve according to expectations [13]. In 1998 Loss and DiVincenzo pointed out that the spin of electron in the semiconductor quantum dot device can be used to prepare qubits, and the spin up and spin down of electrons can be used to encode the qubits $|0\rangle$ and $|1\rangle$ [14]. Petta *et al.* performed a coherent operation on singlet-triplet qubits in the QD system [15]. They used a nuclear magnetic field gradient to achieve coherent oscillation. Manipulating by exchange interaction is easier than single-electron spin qubits, and the magnetic noise associated with causing qubits to be out of phase can be reduced in the semiconductor environment [16–20]. This research mainly

focuses on qubits formed in single and double QD systems, using oscillating magnetic field and dynamic exchange interaction to cause qubit flipping and regulation. We will consider how multiple spins are present to encode qubits with long quantum decoherence time and required fault-tolerant quantum computing [21–25]. Some researchers recently proposed that using resonance theory on the triangle triple quantum dots (TTQDs) encoding qubits has a greater advantage [26–31]. For example, Hsieh and Hawrylak *et al.* proposed a quantum circuit theory based on electron spin to encode qubits in TTQDs, using single chiral qubits for initialization, coherent control, and measurement and implementing a nonlocal two-qubit gate with long coherence time [32].

The TTQDs are the smallest structures that exhibit topological properties, and their inner three spins can be extended into chiral topological angles $\Omega = \hat{S}_1 \cdot (\hat{S}_2 \times \hat{S}_3)$. Previous studies found when the symmetry or external field of half-filling TTQDs is changed, the spin and chiral degrees of freedom are disrupted, resulting in the splitting of mixed quadruple degenerate chiral states [33–36]. In one of the spin subspace, the dominant states will flip with applied bias and vertical magnetic flux. Meanwhile, the TTQDs system will excite clockwise (CW) and counterclockwise (CCW) chiral circulations, corresponding to the CW or CCW chiral states. Further research found that in this topological structure, the chiral current excited within a small bias can be equivalently replaced by the vertical magnetic flux, showing the substitutability of magnetoelectricity [36].

In this paper by comparison of the theoretical derivation and simulation calculation results, we completed the initialization, manipulation, and readout of hybrid qubits in the doubly degenerate chiral ground states. The two chiral states

*yd_wang@ucas.ac.cn

†wjh@ruc.edu.cn

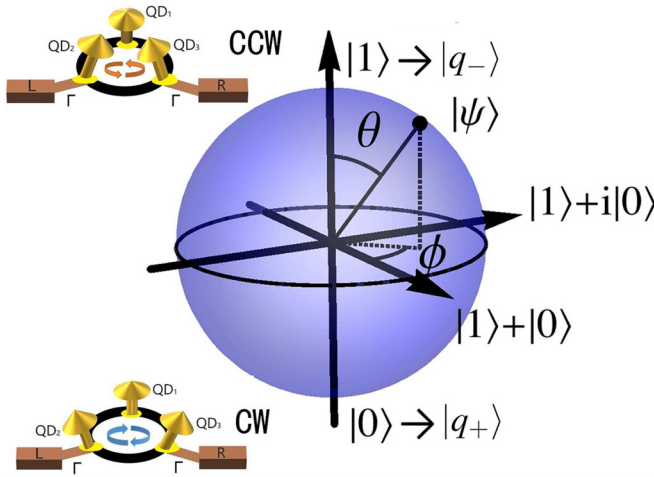


FIG. 1. The chiral states regulate as qubits in the Bloch sphere space, where clockwise (CW) $|q_+\rangle$ and counterclockwise (CCW) $|q_-\rangle$ chiral states split in TTQDs as qubits $|0\rangle$ and $|1\rangle$. The pole and azimuth angle θ and ϕ , expressed as the angle relative to the z axis and x axis, respectively, can specify any state $|\psi\rangle$. Structural diagram of TTQDs connecting two reservoirs with $\Gamma_{L/R} = 0.025$ meV, where the coupling strength between QD_i and QD_j ($i, j = 1 - 3$) is set to t_0 . The system is half-filling, with $S = 1/2$ on each QD.

are equivalent and can be easily regulated by the external bias and magnetic fields to encode qubits [36]. The TTQD is shown in Fig. 1, in which the system is coupled to QD_2 and QD_3 with hybridization $\Gamma_L = \Gamma_R$. During the initialization, we can add vertical magnetic flux or bias to TTQDs. In a fixed bias or equivalent vertical magnetic flux, two chiral states degenerate, keeping the qubit in the CW or CCW chiral state. In addition, both chiral qubits exist stably in the spin subspace, so they are not affected by noise in a uniform vertical magnetic field or bias voltage to realize electronic controlling.

The manipulation of qubits can utilize quasistatic Zeeman field gradients to achieve rapid flipping between chiral states through chiral interactions. The double chiral qubits rotate around the bipole of the Bloch sphere to achieve qubit manipulation. In the simulation process, we use the probability of projection onto a target chiral state to characterize any qubit and found that the occupation probability of chiral states shows the Rabi oscillation. Through further theoretical derivation, we could observe that the Rabi oscillation cycle and amplitude have a qualitative relationship with the internal chirality and the external static Zeeman field gradient. To compare the simulation with the theoretical formula, we get a series of simulation results by hierarchical equations of motion (HEOM) calculation [37], and the oscillation cycle variation trend is in good agreement with theoretical derivation results.

In order to give a convenient readout method, we found that the direction of the internal chiral circulation can characterize the dominant chiral states, while it is difficult to measure the internal circulation directly in the experiment. Therefore, we use the chiral topological blockage effect between conduction and chiral current to read out qubits. The conduction current evolution with time, which can be easily measured [35,38],

is used to characterize the chiral current and read out the dominant chiral qubits.

II. THEORETICAL METHODS

The total Hamiltonian for the quantum open system is

$$H_T = H_{\text{dots}} + H_{\text{res}} + H_{\text{coup}}, \quad (1)$$

where H_{res} represents the Hamiltonian of the electrode part, and we treat the electrode as a giant regular fermion reservoir ensemble with a noninteracting electron gas. The Hamiltonian for the QDs can be represented as

$$H_{\text{dots}} = \sum_{i=1}^3 \epsilon \hat{n}_i + \sum_{j=1}^3 U_j \hat{n}_{j\uparrow} \hat{n}_{j\downarrow} + \sum_{i,j=1}^3 \sum_{s=\uparrow,\downarrow} t_{ij} \hat{d}_{is}^\dagger \hat{d}_{js}. \quad (2)$$

Here $\epsilon = -U/2$ to maintain particle-hole symmetry, and $\hat{n}_{js} = \hat{d}_{js}^\dagger \hat{d}_{js}$ represents the operator of the occupation number on the QD_j , while t_{ij} represents the coupling strength between the QD_i and QD_j . In this work $t_{ij} = t_0$ is taken to ensure the TTQD symmetry.

Under the vertical magnetic field, the original second-order perturbation theory is no longer applicable, and a third-order superexchange interaction needs to be introduced [39–42]. By perturbing the electron exchange coupling t_{ij} in H_{dots} , we obtain the following effective Hamiltonian [43–45]:

$$H_{\text{eff}} = -t(1-n) \sum_{jk,s} (\hat{d}_{js}^\dagger \hat{d}_{ks} + \text{H.c.}) + J \sum_{j<k} \left(\hat{S}_j \hat{S}_k - \frac{1}{4} \hat{n}_j \hat{n}_k \right) + \chi \hat{S}_1 (\hat{S}_2 \times \hat{S}_3). \quad (3)$$

The third term is the chiral interaction term, the operator of the chiral interaction is $\hat{S}_1 \cdot (\hat{S}_2 \times \hat{S}_3)$, and the chiral coefficient is $\chi = 24t_{12}t_{13}t_{23} \sin(2\pi\Phi/\Phi_0)/U^2$, where Φ is the flux passing through the TTQD.

The electrode is regarded as a free electron gas without interaction, so

$$H_{\text{res}} = \sum_{\alpha \in L,R} \sum_{\kappa s} (\epsilon_{\alpha\kappa s} + \mu_\alpha) \hat{c}_{\alpha\kappa s}^\dagger \hat{c}_{\alpha\kappa s}, \quad (4)$$

with $\mu_L = eV/2 = -\mu_R$. $\epsilon_{\alpha\kappa s}$ is the energy of the electrode electrons in the state of the α -electrode, κ -momentum, and s -spin, and $\hat{c}_{\alpha\kappa s}^\dagger$ and $\hat{c}_{\alpha\kappa s}$ are the generation annihilation operators of the electron in the reservoir, respectively. The decoherence part of chiral qubits is mainly defined by this part. The TTQDs system-reservoir coupling is described as $H_{\text{coup}} = \sum_{\kappa s} (t_{L2} \hat{c}_{L\kappa s}^\dagger \hat{d}_{2s} + t_{R3} \hat{c}_{R\kappa s}^\dagger \hat{d}_{3s} + \text{H.c.})$, and the linear coupling coefficient between the quantum dot and electrode is t_{L2} , t_{R3} is the coupling coefficient between QD_2 and the left electrode, and the coupling coefficient between QD_3 and the right electrode, respectively, thus forming the coupling matrix.

The HEOM approach investigates the properties of quantum dots in both equilibrium and nonequilibrium states via the reduced density operator, which has a universal formalism for an arbitrary system Hamiltonian; thus, it can be used to accurately solve the three-impurity Anderson model [41]. The HEOM approach is established based on Feynman-Vernon influence functional path-integral theory [46] without any approximations, and implemented with Grassmann algebra for

fermion dissipations [47]. Basically, the HEOM is a non-perturbative method for general quantum systems coupled to reservoir baths that satisfy Grassmann Gaussian statistics. The reduced density matrix and a set of auxiliary density matrices are the basic variables in HEOM. Basing on the linear response theory of quantum open systems, the HEOM can obtain dynamical observables of strongly correlated quantum impurity systems accurately and efficiently [41,48]. At time t , the reduced system density operator, $\rho(t) = \text{tr}_{\text{res}} \rho_{\Gamma}(t)$, is related to the initial value at time t_0 via the reduced Liouville-space propagator $\mathcal{G}(t, t_0)$ by

$$\rho(t) = \mathcal{G}(t, t_0)\rho(t_0). \quad (5)$$

The influence of bath enters the equations of motion with M exponentiations. The auxiliary density operators (ADOs) $\{\rho_j^n = \rho_{j_1 \dots j_n}\}$ are determined by the time derivative of the influence functional. The final form can be reduced to the following compact form (the detailed derivation process can be found in the Appendix):

$$\begin{aligned} \dot{\rho}_{j_1 \dots j_n}^{(n)} = & - \left(i\mathcal{L} + \sum_{r=1}^n \gamma_{j_r} \right) \rho_{j_1 \dots j_n}^{(n)} - i \sum_j \mathcal{A}_{j\bar{j}} \rho_{j_1 \dots j_n, j}^{(n+1)} \\ & - i \sum_{r=1}^n (-)^{n-r} C_{j_r} \rho_{j_1 \dots j_{r-1} j_{r+1} \dots j_n}^{(n-1)}. \end{aligned} \quad (6)$$

In a three-spin TTQD system, there are two subspaces: one is the space with total spin $S_{\text{tot}} = 3/2$, the other is a subspace whose total spin is $S_{\text{tot}} = 1/2$. Considering the subspace $S_z = -1/2$, the chirality degenerate states split into CW and CCW chiral states [36]: $|q_{\pm}^{-1/2}\rangle = \frac{1}{\sqrt{3}}(|\uparrow\downarrow\downarrow\rangle + e^{\pm \frac{i2\pi}{3}}|\downarrow\uparrow\downarrow\rangle + e^{\pm \frac{i4\pi}{3}}|\downarrow\downarrow\uparrow\rangle)$. The chiral current occurs, whose magnitude is approximately equal to the conduction current between QDs, $\hat{J}_{\alpha=L/R}(t) = \hat{J}_t = i \sum_{\mu s} \text{tr}[\rho_{\alpha\mu s}^\dagger(t) \hat{d}_{\mu s} - \hat{d}_{\mu s}^\dagger \rho_{\alpha\mu s}(t)]$. We can define the chiral current using the Feynman-Hellman theorem [41,46,49,50]:

$$\hat{J}_c = -\frac{e}{\hbar} \left\langle \frac{\partial \hat{H}_{\text{dots}}}{\partial \phi} \right\rangle = -\frac{24e}{\hbar} \frac{t_{12} t_{13} t_{23}}{U^2} (\hat{S}_1 \cdot (\hat{S}_2 \times \hat{S}_3)). \quad (7)$$

In this $S_z = -1/2$ subspace, the Hamiltonian of the two-state $|q_{\pm}^{-1/2}\rangle$ in the TTQDs system is given as (see Appendix for detailed derivation process) [50,51]

$$H_{Bz} = \begin{pmatrix} E_0 + \chi & W_1 + iW_2 \\ W_1 - iW_2 & E_0 - \chi \end{pmatrix}, \quad (8)$$

where B_{z_i} ($i = 1 - 3$) represents the additional local Zeeman field on the QD_i :

$$\begin{aligned} E_0 &= -(B_{z1} + B_{z2} + B_{z3}) - J, \\ W_1 &= 2B_{z1} - B_{z2} - B_{z3}, \\ W_2 &= \sqrt{3}i(B_{z2} - B_{z3}). \end{aligned} \quad (9)$$

The eigenvalues of this matrix are given by

$$\begin{aligned} E_+ &= E_0 + \sqrt{W_1^2 + W_2^2 + \chi^2}, \\ E_- &= E_0 - \sqrt{W_1^2 + W_2^2 + \chi^2}, \end{aligned} \quad (10)$$

and $|W| = \sqrt{W_1^2 + W_2^2}$. The probability that TTQDs system in the state $|q_+\rangle$ will be found in the arbitrary state

$$P_{q_+ \rightarrow q_+}(t) = \rho_{q_+ q_+} = 1 - \frac{|W|^2}{\chi^2 + |W|^2} \sin^2 \left(\frac{(E_+ - E_-)t}{2\hbar} \right). \quad (11)$$

Therefore, Rabi oscillations in chiral two-level systems can be achieved by adding nonuniform static Zeeman fields to TTQDs. Equation (11) is called the Rabi formula, showing the probability oscillation with angular frequency.

III. RESULTS AND DISCUSSION

A. Initialization chiral qubits in TTQDs

According to the previous study in TTQDs system [36], magnetoelectric regulation between the two chiral states is equivalent. In the small bias range, the chiral term caused by the bias can be replaced by the vertical magnetic flux, which is called the equivalent magnetic flux. As shown in Fig. 2(a), the J_c as functions of bias ($-0.06 < V < 0.06$ mV) and vertical magnetic flux have the same changing tendency. The equivalent magnetic flux acts as a function of bias ($-0.05 < V < 0.05$ mV) with the same chiral term in circular TTQDs and are shown in the figure. The corresponding relationship between the bias and equivalent magnetic flux is approximately linear. By adding bias or vertical magnetic flux to the TTQDs, we can split the double degenerate chiral states $|q_{\pm}\rangle$ in spin $S_z = -1/2$ subspace.

In the initialization, we mainly study the TTQDs under C_{3v} symmetry with $t_0 = 0.25$ meV. The TTQD is weakly coupled with lead $\Gamma_L = \Gamma_R = 0.01$ meV and the temperature set as $k_B T = 0.02$ meV. As shown in Fig. 2(b), when we add the magnetic flux $\Phi/\Phi_0 = 0.06$ perpendicular to the TTQD ring at the initial time $t = 0$ ps, the occupancy probability of the two chiral states $|q_{\pm}^{-1/2}\rangle$ changes with the evolution time. We can see when the vertical magnetic flux is added to the system, the two chiral states split at the initial time and can remain stable for a long time. Here only the evolution graphs of the reduced density matrix diagonal elements of the two chiral states over time t are given when the evolution time is up to 6000 ps. Ultimately, the difference between the two chiral states is $\rho_{q_+ q_+} - \rho_{q_- q_-} = 0.32$, which is enough for the two quantum states to achieve complete separation in the $S_z = 1/2$ subspace, thus preparing two initial qubits to accomplish initialization.

At the same time, when we add the bias in TTQDs at the initial time $t = 0$ ps, the evolution of the occupancy probability of the two chiral states over time is shown in Fig. 2(c). When we initialize the TTQDs with pure electricity, the two chiral states $|q_{\pm}\rangle$ will degenerate at $t = 0$ ps, with populations $\rho_{q_+ q_+} = \rho_{q_- q_-}$. As we apply bias $V = 0.05$ to the TTQDs, the two chiral states split with the evolution time. The difference between the occupation probabilities becomes larger with t and finally reaches stabilization at $t = 6000$ ps with $\rho_{q_+ q_+} - \rho_{q_- q_-} = 0.2$. Therefore, in the initialization, we can add vertical magnetic flux or external bias to the TTQDs at the initial evolution time $t = 0$ ps. Both initialization methods can split the two chiral states sufficiently in spin subspace to

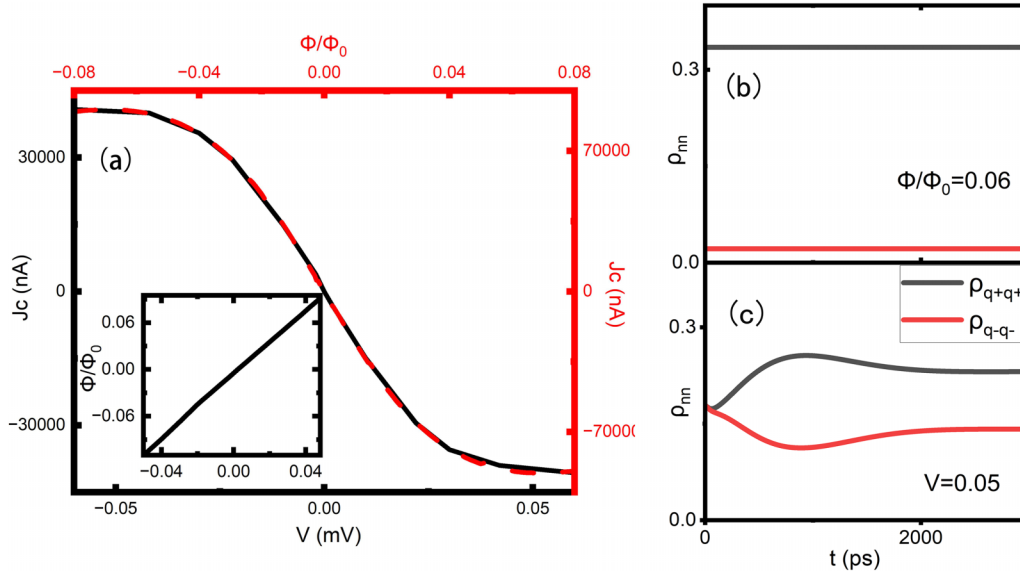


FIG. 2. (a) In the small bias range (-0.06 mV to 0.06 mV), comparison of the chirality due to the bias (black line) and vertical magnetic flux (red line). The TTQDs is in symmetrical configuration, $t_0 = 0.25$ meV, $\Gamma = 0.01$ meV, $\epsilon = -U/2 = -0.5$ meV, under $k_B T = 0.02$ meV. The illustration is a fitting of the equivalent magnetic flux and bias. (b) When the vertical magnetic flux $\Phi/\Phi_0 = 0.06$ is used for initialization, the occupancy probability of the two chiral states (ρ_{nm}) changes with the evolution time. The population probability of the CW chiral state (ρ_{q+q+}) is shown by the red curve, and the CCW chiral state (ρ_{q-q-}) is the black line. (c) When the bias $V = 0.05$ mV is applied in the TTQDs to achieve initialization, the occupancy probability of the two chiral states changes with t . The unit of evolution time is set to the ps.

prepare two stable initial qubits on the Bloch sphere, where $|q_+^{-1/2}\rangle$ acts as qubit $|0\rangle$ and $|q_-^{-1/2}\rangle$ as qubit $|1\rangle$.

B. Manipulation the chiral qubits in TTQDs

Next, we study the qubit manipulation process in TTQDs system. According to theoretical derivation, we get that the qubit regulation can be simulated by adding static a nonuniform Zeeman field to the QDs in a chiral two-level system. At time t , the probability of CW chiral state $|q_+^{-1/2}\rangle = |0\rangle$ is represented as Eq. (13). In order to simplify the formula, we make the Zeeman field in the z direction added onto QD_2 and QD_3 the same, and add different fields on QD_1 to achieve the Zeeman field gradient, with $B_{z2} = B_{z3} \neq B_{z1}$. So $W_2 = 0$, and the Rabi oscillation amplitude and cycle between the two chiral states can be expressed:

$$A_{q_+ \rightarrow q_+}(t) = A = \frac{4(B_{z1} - B_{z2})^2}{4(B_{z1} - B_{z2})^2 + \chi^2}, \quad (12)$$

$$T = \frac{2\pi\hbar}{\sqrt{4(B_{z1} - B_{z2})^2 + \chi^2}}, \quad (13)$$

which is called the Rabi oscillation. Thus, qubit oscillation between $|0\rangle$ and $|1\rangle$ states can be manipulated by adding a nonuniform Zeeman field to QD_1 and QD_2 or by changing the internal chiral interaction term χ in TTQDs.

As shown in Fig. 3, we add nonuniform Zeeman fields with different gradients ($\Delta B_z = 0.01, 0.02, 0.04$) to the TTQDs after the initialization $t = 3000$ ps; the two chiral states' population $|q_{\pm}\rangle$ are functions of the evolution time t . We find that with the increase of the gradient $\Delta B_z = B_{z1} - B_{z2}$, the

oscillation frequency of the two chiral states' occupation probability $\rho_{q_{\pm}q_{\pm}}$ will also accelerate, corresponding to the shorter period of the Rabi oscillation, while the oscillation amplitude is not significantly changed. This corresponds well to the qualitative trend of formulas (16) and (17).

As shown in Fig. 3(a), when the Zeeman field gradient $\Delta B_z = 0.01$ is added, the oscillation frequency of two chiral states is slow and decays quickly. Near $t = 4000$ ps, the two chiral states are gradually decohered, thus qubit regulation cannot be realized. However, with the increase of the Zeeman fields' gradient ($\Delta B_z = 0.02, 0.04$), the oscillations of the two qubits are accelerated and the decoherence time is longer, which is shown in in Figs. 3(b)–3(d). As shown in Fig. 3(b), when the magnetic field gradient is 0.02, the decoherence time can be extended to $t = 5000$ ps. The oscillation of two chiral states' occupancy probability is further accelerated at $\Delta B_z = 0.04$, seen in Figs. 3(c) and 3(d), and the decoherence time can be extended to around $t = 8000$ ps. Before this, the two-state system evolved a nearly perfect Rabi oscillation. The time evolution of the two chiral states' occupation probability is enlarged at $t = 2800$ – 3200 ps, shown in Fig. 3(d). The Rabi flipping of the two chiral states is realized at the end of initialization ($t = 3000$ ps) by the nonuniform Zeeman field ΔB_z . This further demonstrates that Rabi oscillations of qubits $|0\rangle$ and $|1\rangle$ on Bloch sphere can be achieved by adding ΔB_z to TTQDs, while the oscillation cycle of qubits and decoherence time is closely related to the magnitude of ΔB_z .

In order to verify the relationship between the Rabi cycle and Zeeman field gradient ΔB_z in formula (17), we consider only the evolution of the CW chiral state occupation population as time in different Zeeman field gradient $\Delta B_z = 0.02$ (red curve), $\Delta B_z = 0.03$ (blue curve), $\Delta B_z = 0.04$ (green

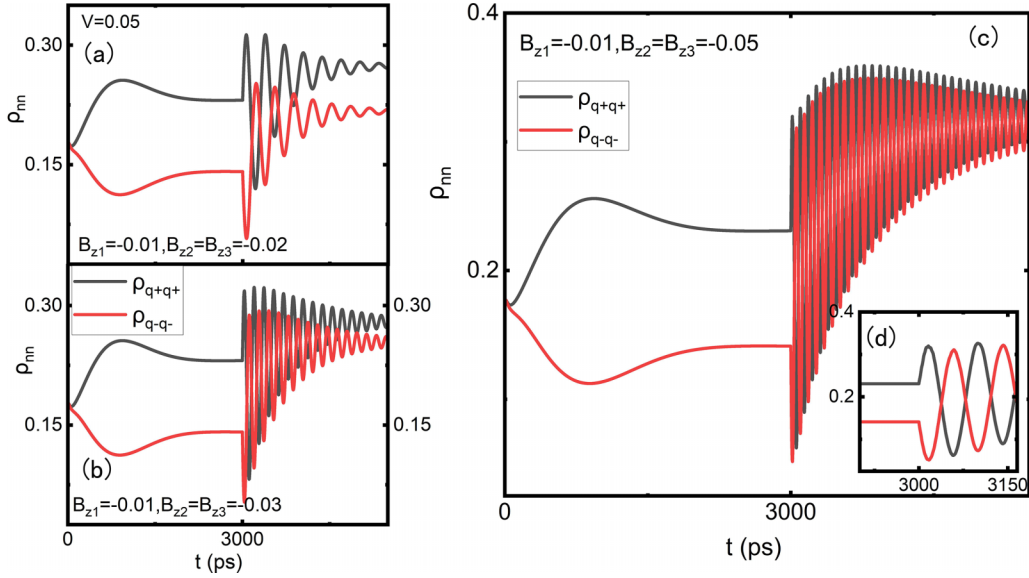


FIG. 3. After the initialization ($t = 0 - 3000$ ps) with bias $V = 0.05$ mV, a constant Zeeman field gradient $\Delta B_z = B_{z1} - B_{z2}$ is added at $t = 3000$ ps. When $B_{z1} = -0.01$, $B_{z2} = -0.02$ and Zeeman field gradient $\Delta B_z = 0.01$, the evolution of the two chiral states' population $\rho_{q\pm q\pm}$ with the time t is shown (a). When the Zeeman field gradient increases to $\Delta B_z = 0.02$ ($B_{z1} = -0.01$, $B_{z2} = -0.03$), the evolution of the two chiral states' population with time after $t = 3000$ ps is shown (b). (c, d) As ΔB_z increases to 0.04 ($B_{z1} = -0.01$, $B_{z2} = -0.05$), the two chiral states' population are as functions of t . We capture the evolution process of $t = 2800 - 3200$ to enlarge (c), which is shown as (d). The TTQDs system maintains equilateral symmetry, and the other parameters remain unchanged.

curve), and $\Delta B_z = 0.05$ (purple curve), as shown in Fig. 4(a). At this time, we fixed the TTQDs structure unchanged as above and obtained that the internal chiral term under steady state is $\chi = -38$ meV. As the ΔB_z increases, it can be seen that the Rabi cycle gradually shrinks. For quantitatively comparing the results of theoretical and HEOM calculations, we obtained the the Rabi cycle of HEOM simulations (red curve) and theoretical calculations (black curve) under different ΔB_z from a series of images, as shown in Fig. 4(b). We can see that the two results fit well, which further proves that in TTQDs, the qubits can be controlled directionally for a long time by an externally ΔB_z . Moreover, these chiral qubits have strong stability and controllability in the topological structure, which can resist the influence of external noise on qubits to regulate with a long decoherence time.

In addition, from formula (17), we can also find that the Rabi cycle is also related to the internal chiral interaction term χ of TTQDs. Therefore, we also calculate the evolution of the Rabi oscillation with time when only the Coulomb repulsive interaction ($U = -2\epsilon = 0.8, 1, 1.2$ meV) of TTQDs is changed and other parameters remain unchanged, as seen in Fig. 5(a). When the Coulomb repulsion energy between QDs is $U = -2\epsilon = 0.8$ meV (black curve), the steady-state chiral interaction of the TTQD is $\chi = -28.3$ meV, and in $U = -2\epsilon = 1$ and $U = -2\epsilon = 1.2$ meV, the chiral interaction term becomes larger, which is $\chi = -37.4$ and $\chi = -57.8$ meV, respectively. With the increase of the chiral interaction, the Rabi cycle is correspondingly shortened, obtained by simulation as 240, 250, and 270, ps respectively. We also compare the theoretical formula (17) and HEOM calculation, and the Rabi cycle changes with different chiral terms χ and the two results

can also be well fitted, as shown in Fig 5(b). This also verifies that in TTQDs, it is possible to realize the Rabi oscillation of the two chiral states system as qubits by regulating both ΔB_z and the internal chiral terms χ . Moreover, the specific manipulation of the Rabi cycle and amplitude can be predicted by formulas (16) and (17), thus achieving qubit manipulation in the Bloch sphere.

C. Readout of chiral qubits

In this part, we discuss the readout of chiral qubits. The direction of the chiral circulation can represent the corresponding output chiral state at this time; that is, if the chiral current direction is CW, then $J_c < 0$ corresponds to the chiral state $|q_+\rangle$ as qubit $|0\rangle$. When $J_c > 0$, the chiral current direction transforms into CCW and the dominant chiral state $|q_-\rangle$ as qubit $|1\rangle$. However, the chiral circulation is an internal effect of TTQDs, and it is difficult to measure in experiment. Considering the blocking relationship between the conduction current J_t and the chiral current J_c , we propose to use the easily measured J_t evolution to characterize the J_c , so as to read out the dominant chiral qubits at this time.

As shown in Fig. 6, we give the evolution of J_c and J_t with time under $\Delta B_z = 0.01$ (black curve) and $\Delta B_z = 0.02$ (red curve). We find that the overall change trend of J_c is similar to J_t . When $\Delta B_z = 0.01$, the Rabi oscillation cycle is relatively large, seen in Fig. 6(a). At this time, when the evolution time $t = 3080$ ps, the chiral current flip point appears. In $t = 3000 - 3080$ ps, $J_c < 0$, and the direction of chiral circulation is CW corresponding to the dominant state is $|q_+\rangle$,

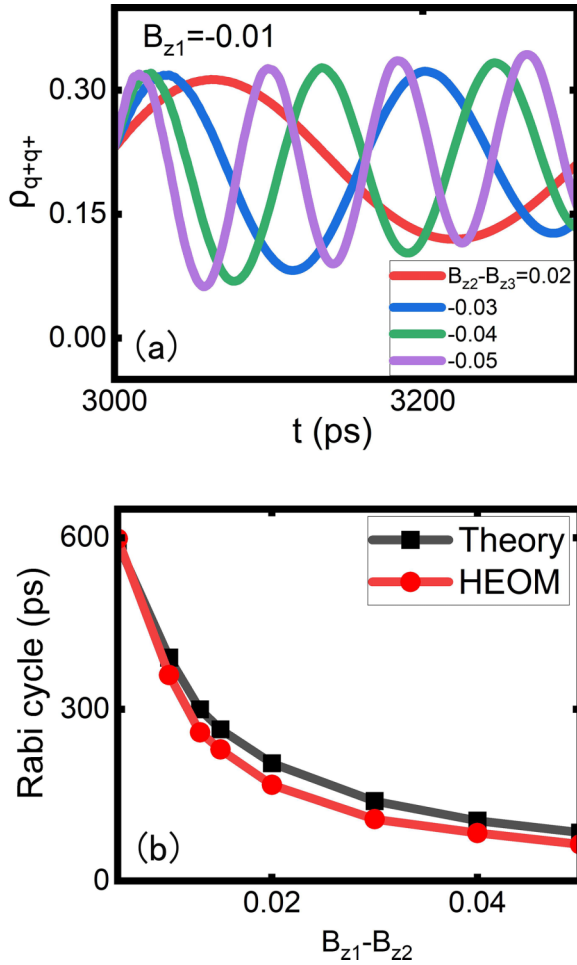


FIG. 4. (a) After initialization, the TTQD system is added with different magnetic gradients ($\Delta B_z = 0.01, 0.02, 0.03, 0.04$), and the evolution of the CW chiral state $|q_+\rangle = |0\rangle$ occupation probability is within $t = 3000$ – 3300 ps. Other system parameters must be consistent with those described above. (b) The Rabi cycle is calculated as a function of ΔB_z by theoretical equation (17) and HEOM simulations.

while in $t = 3080$ – 3240 ps, chiral circulation transforms into CCW, $J_c > 0$, corresponding to $|q_-\rangle$. As for $\Delta B_z = 0.02$, the Rabi cycle gets shorter as ΔB_z gets larger with the transition point $t = 3040$ ps. In $t = 3000$ – 3040 ps, chiral circulation is CW, $J_c < 0$, and reads out as $|q_+\rangle$, while in $t = 3040$ – 3160 ps, $J_c > 0$ as $|q_-\rangle$.

The trend of the J_t is approximately the same as that of J_r after initialization $t_1 = 3000$ ps, shown in Fig. 6(b). We find that the peak value of J_c over time t is easy to find, defined as t_{\max} , corresponding to half of the time between $t_1 = 3000$ and the peak value, $t_s = (t_{\max} - t_1)/2$, that is, the reversal time of the chiral circulation. In the evolution time $t_1 < t < t_s$, the internal dominant chiral state is $|q_+\rangle$, and the subsequent $t_s < t < 3t_s$ is $|q_-\rangle$, where the readout qubit is respectively $|0\rangle$ or $|1\rangle$. Therefore, we can easily measure the evolution of the conduction current over time in the experiment so as to obtain the corresponding chiral circulation trend to determine the reversal time t_s . Using the chiral topological frustration effect, we can fix the chiral state at any time and readout the chiral qubits in TTQDs.

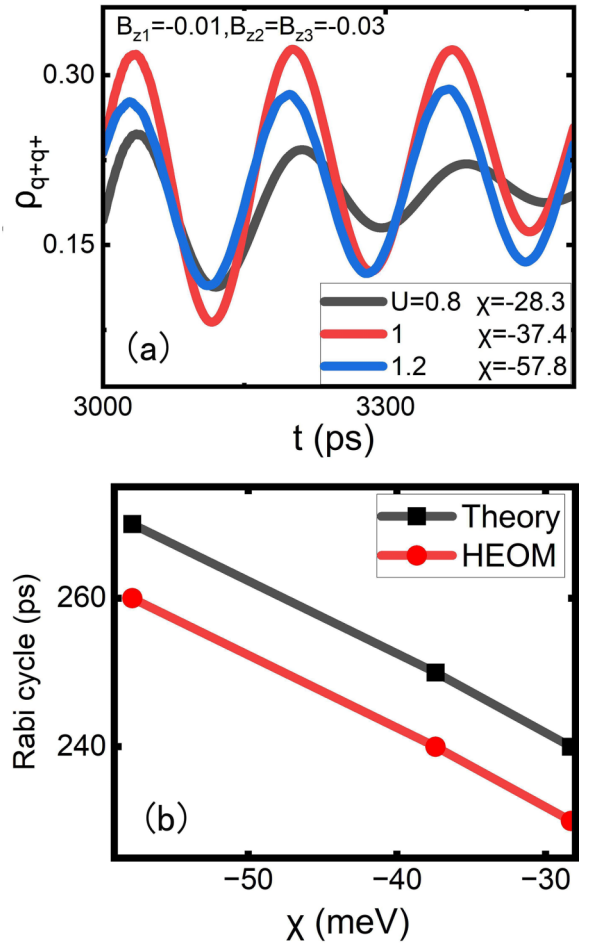


FIG. 5. (a) In TTQDs, when different Coulomb repulsion energy ($U = -2\epsilon = 0.8, 1, 1.2$ meV) carries different chiral terms, the evolution of CW chirality with time t . (b) The Rabi cycle is calculated as a function of χ by theoretical equation (17) and HEOM simulations. Other parameters are consistent with those above.

IV. DISCUSSION

If an inhomogeneous charge noise is introduced to a single quantum dot, rapid decoherence is induced. For example, Weymann used the real-time diagrammatic technique up to the second order to determine the conductance and charge noise in a triangular triple quantum dot system [52]. It is found that in the transport state of dark state and Coulomb blocking, the charge noise is usually hyper-Poisson, the chiral blocking can be relieved by the cotunneling process, and the corresponding Fano factor is reduced. However, the qualitative results in this paper are not affected by the charge noise acting on single quantum dot. The decoherence time can still be maintained, and the chiral qubit can be manipulated by adjusting the external bias and the internal chiral interaction.

V. SUMMARY

In conclusion, we propose an alternative chiral qubit model in the TTQD topological structure. According to previous studies, the internal chiral interaction can be stimulated by applying vertical magnetic flux or bias voltage, presenting

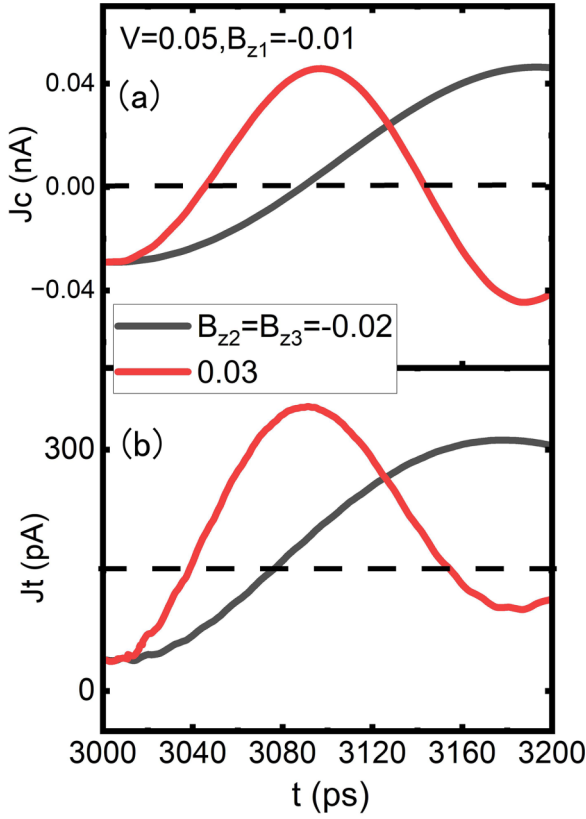


FIG. 6. (a) In TTQDs, when $B_{z1} = -0.01$, $B_{z2} = -0.02$ (black curve) and $B_{z1} = -0.01$, $B_{z2} = -0.03$ (red curve), the evolution of chiral current J_c with time t , and (b) the evolution of conduction current J_t with time t . Other parameters are consistent with those above.

chiral states from splitting. We use this minimized topology to initialize chiral qubits by the bias voltage. In the manipulation, we added a nonuniform Zeeman field in TTQDs to make the chiral qubits' oscillation. The Rabi cycle of the theoretical formula and the simulation results fit well, which further proves that qubit manipulation in TTQDs is feasible and controllable. Finally, we use the chiral topological blockage effect to characterize the chiral current by the conduction current changes so as to realize the qubit readout. The qubit initialization, manipulation, and readout based on the smallest topological ring can be realized in the experiment, which has a certain guiding role for the experiment.

ACKNOWLEDGMENTS

We acknowledge support from the Natural Science Foundation of China (Grants No. 12274454, No. 11774418, No. 11374363, No. 11674317, No. 11974348, No. 11834014, and No. 21373191), the Strategic Priority Research Program of CAS (Grants No. XDB28000000 and No. XDB33000000), NSFC (Grant No. 11974348), and the Training Program of Major Research plan of NSFC (Grant No. 92165105). This work is supported by the Outstanding Innovative Talents Cultivation Funded Programs 2023 of Renmin University of China. The computational resources have been provided by

the Physical Laboratory of High Performance Computing at Renmin University of China.

APPENDIX

1. Anderson impurity model

The total system Hamiltonian which can be described by the Anderson impurity model is [33,53,54]

$$H_T = H_{\text{dots}} + H_{\text{res}} + H_{\text{coup}}. \quad (\text{A1})$$

The TQD system-reservoir coupling is described as Eq. (4). The linear coupling coefficient between quantum dot and electrode is t_{L2} , t_{R3} is the coupling coefficient between QD2 and the left electrode, and the coupling coefficient between QD3 and the right electrode, respectively, thus forming the coupling matrix. $\hat{c}_{\alpha\kappa s}^\dagger$ in the first term represents the generation operator of the state on the left electrode. \hat{d}_{2s} denotes the annihilation operator on QD2, and in the second term corresponds to the generation operator of the state on the right electrode and the annihilation operator on QD3.

2. The theoretical derivation of manipulating qubits

When the Zeeman field is applied, the Hamiltonian of the system can be written as Eq. (3). In order to simplify, we set $\epsilon = -U/2 = -0.5$ meV to keep the system in the particle-hole symmetry that each QD is half-filling with the occupation $n = 1$, and the first term reduces to zero:

$$H_{Bz} = \sum_{\alpha=1-3} g\mu_B S_\alpha B + J \sum_{j<k} \left(\hat{S}_j \hat{S}_k - \frac{1}{4} \hat{n}_j \hat{n}_k \right) + \chi \hat{S}_1 (\hat{S}_2 \times \hat{S}_3), \quad (\text{A2})$$

$$\chi = 24t_{12}t_{13}t_{23} \sin(2\pi\phi/\phi_0)/U^2. \quad (\text{A3})$$

In the $S_z = -1/2$ subspace, the quadruplet states degenerate into clockwise (CW) and counterclockwise (CCW) chiral states $|q_{\pm}^{-1/2}\rangle = \frac{1}{\sqrt{3}}(|\uparrow\downarrow\downarrow\rangle + e^{\pm\frac{i2\pi}{3}}|\downarrow\uparrow\downarrow\rangle + e^{\pm\frac{i4\pi}{3}}|\downarrow\downarrow\uparrow\rangle)$:

$$H_{11} = \langle q_+^{-1/2*} | H_{Bz} | q_+^{-1/2} \rangle = -(B_{z1} + B_{z2} + B_{z3}) - J + \chi, \quad (\text{A4})$$

$$H_{22} = \langle q_-^{-1/2*} | H_{Bz} | q_-^{-1/2} \rangle = -(B_{z1} + B_{z2} + B_{z3}) - J - \chi, \quad (\text{A5})$$

$$H_{12} = \langle q_+^{-1/2*} | H_{Bz} | q_-^{-1/2} \rangle = 2B_{z1} - B_{z2} - B_{z3}, \quad (\text{A6})$$

$$H_{21} = \langle q_-^{-1/2*} | H_{Bz} | q_+^{-1/2} \rangle = H_{12} = 2B_{z1} - B_{z2} - B_{z3}. \quad (\text{A7})$$

The Hamiltonian can be expressed by the spin Pauli matrix as

$$H_{Bz} = E_0\sigma_0 + W_1\sigma_x - W_2\sigma_y + \chi\sigma_z, \quad (\text{A8})$$

and let

$$\begin{aligned}\sin \theta &= \frac{|W|}{\sqrt{W_1^2 + W_2^2 + \chi^2}}, \\ \cos \theta &= \frac{\chi}{\sqrt{W_1^2 + W_2^2 + \chi^2}}, \\ \tan \theta &= \frac{|W|}{\chi}.\end{aligned}\quad (\text{A9})$$

Now, eigenvectors for E_+ and E_- can be found from

$$|E_+\rangle = \begin{pmatrix} \cos(\theta/2) \\ e^{i\phi} \sin(\theta/2) \end{pmatrix} \quad (\text{A10})$$

and

$$|E_-\rangle = \sin\left(\frac{\theta}{2}\right)|q_+\rangle - e^{i\phi} \cos\left(\frac{\theta}{2}\right)|q_-\rangle. \quad (\text{A11})$$

So

$$|q_+\rangle = \cos\left(\frac{\theta}{2}\right)|E_+\rangle + \sin\left(\frac{\theta}{2}\right)|E_-\rangle, \quad (\text{A12})$$

$$|q_-\rangle = e^{-i\phi} \cos\left(\frac{\theta}{2}\right)|E_+\rangle - e^{-i\phi} \sin\left(\frac{\theta}{2}\right)|E_-\rangle. \quad (\text{A13})$$

Suppose the system starts in state q_+ at time $t = 0$,

$$|\psi(0)\rangle = |q_+\rangle = \cos\left(\frac{\theta}{2}\right)|E_+\rangle + \sin\left(\frac{\theta}{2}\right)|E_-\rangle. \quad (\text{A14})$$

After time t , the state evolves as

$$\begin{aligned}|\psi(t)\rangle &= e^{-\frac{i\hat{H}t}{\hbar}}|q_+\rangle \\ &= e^{-\frac{i\hat{H}t}{\hbar}}|\psi(0)\rangle \\ &= \cos\left(\frac{\theta}{2}\right)e^{-\frac{iE_+t}{\hbar}}|E_+\rangle + \sin\left(\frac{\theta}{2}\right)e^{-\frac{iE_-t}{\hbar}}|E_-\rangle \\ &= \left[(\cos\theta - 1) \left(\sin\frac{(E_+ - E_-)t}{2\hbar} e^{-\frac{i(E_+ + E_-)t}{2\hbar}} \right) |q_+\rangle \right. \\ &\quad \left. + \sin\theta \left(\sin\frac{(E_+ - E_-)t}{2\hbar} e^{-\frac{i(E_+ + E_-)t}{2\hbar}} \right) e^{i\phi} |q_-\rangle \right] \\ &= e^{-\frac{i(E_+ + E_-)t}{2\hbar}} \left(\cos\frac{(E_+ - E_-)t}{2\hbar} \right. \\ &\quad \left. - i \cos\theta \sin\frac{(E_+ - E_-)t}{2\hbar} \right) |q_+\rangle \\ &\quad + e^{-\frac{i(E_+ + E_-)t}{2\hbar}} \left(-i \sin\theta \sin\frac{(E_+ - E_-)t}{2\hbar} \right) e^{i\phi} |q_-\rangle \\ &= e^{-i\alpha t/\hbar} (\cos\beta |q_+\rangle + \sin\beta e^{i\phi} |q_-\rangle) \\ &= U(t) (\cos\beta |q_+\rangle + \sin\beta e^{i\phi} |q_-\rangle). \quad (\text{A15})\end{aligned}$$

The matrix $\mathbf{U}(t)$ is called the time evolution matrix (which comprises the matrix elements of $\alpha = \frac{E_+ + E_-}{2} = E_0$). It is easily proved that $\mathbf{U}(t)$ is unitary, meaning that $\mathbf{U}^\dagger \mathbf{U} = 1$.

The probability amplitude of finding the system at time t in the state q_- is given by

$$\langle q_- | \psi(t) \rangle = e^{i\phi} \sin\left(\frac{\theta}{2}\right) \cos\left(\frac{\theta}{2}\right) \left(e^{-\frac{iE_+t}{\hbar}} - e^{-\frac{iE_-t}{\hbar}} \right), \quad (\text{A16})$$

and the probability that a system in the state $|\psi(t)\rangle$ will be found to be in the arbitrary state q_- is given by

$$P_{q_+ \rightarrow q_-}(t) = \frac{|W|^2}{\chi^2 + |W|^2} \sin^2\left(\frac{(E_+ - E_-)t}{2\hbar}\right). \quad (\text{A17})$$

At the same time, the oscillation amplitude

$$A_{q_+ \rightarrow q_+}(t) = \sin^2(\theta) = \frac{|W|^2}{\chi^2 + |W|^2} = \frac{W_1^2 + W_2^2}{W_1^2 + W_2^2 + \chi^2}. \quad (\text{A18})$$

We set $B_{z2} = B_{z3}$, so $W_2 = 0$ and

$$A_{q_+ \rightarrow q_+}(t) = A = \frac{4(B_{z1} - B_{z2})^2}{4(B_{z1} - B_{z2})^2 + \chi^2}. \quad (\text{A19})$$

Taking arbitrary phase angle ϕ , we can write

$$\begin{aligned}\exp(i\phi) &= \frac{1}{\tan\frac{\theta}{2}} \frac{\chi - \sqrt{W_1^2 + W_2^2 + \chi^2}}{W_1 + iW_2} \\ &= \frac{1}{W_1 + iW_2} \frac{\sqrt{A} - \sqrt{\frac{A}{1-A}}}{\sqrt{A} - \sqrt{1-A}} \\ &= \frac{1}{W} \frac{\sqrt{A(1-A)} - \sqrt{A}}{\sqrt{A(1-A)} - (1-A)}. \quad (\text{A20})\end{aligned}$$

The probability is oscillatory with angular frequency

$$\omega = \frac{E_+ - E_-}{2\hbar} = \frac{\sqrt{\chi^2 + |W|^2}}{\hbar} = \frac{\sqrt{4(B_{z1} - B_{z2})^2 + \chi^2}}{\hbar}, \quad (\text{A21})$$

which is simply the unique Bohr frequency of the system and also called the Rabi frequency.

3. The detailed derivation for the HEOM approach

The HEOM approach investigates the properties of quantum dots in both equilibrium and nonequilibrium states via the reduced density operator, which has a universal formalism for an arbitrary system Hamiltonian; thus, it can be used to accurately solve the three-impurity Anderson model [41,44,50,51,55]. The HEOM approach is established based on Feynman-Vernon influence functional path-integral theory [46] without any approximations, and implemented with Grassmann algebra for fermion dissipations [47]. Basically, the HEOM is a nonperturbative method for general quantum systems coupled to reservoir baths that satisfy Grassmann Gaussian statistics. The reduced density matrix and a set of auxiliary density matrices are the basic variables in HEOM. Based on the linear response theory of quantum open systems, the HEOM can obtain dynamical observables of strongly correlated quantum impurity systems accurately and efficiently [41,48].

Let $|\psi\rangle$ be an arbitrary basis set defined in system space, and $\boldsymbol{\psi} = (\psi, \psi')$. Therefore $\rho(\boldsymbol{\psi}, t) = \rho(\psi, \psi', t)$. From the Feynman-Vernon influence functional, the path-integral expression for the reduced Liouville-space propagator is

$$\mathcal{G}(\boldsymbol{\psi}, t; \boldsymbol{\psi}_0, t_0) = \int_{\boldsymbol{\psi}_0[t_0]}^{\boldsymbol{\psi}[t]} \mathcal{D}\boldsymbol{\psi} e^{iS[\boldsymbol{\psi}]} \mathcal{F}[\boldsymbol{\psi}] e^{-iS[\boldsymbol{\psi}']}. \quad (\text{A22})$$

Here $S[\boldsymbol{\psi}]$ is the classical action of the reduced system. $\mathcal{F}[\boldsymbol{\psi}]$ is the influence functional determined by the Grassmann variables of the system-environment coupling $f_{\alpha is}^\dagger(t) d_{is}[\boldsymbol{\psi}] + \text{H.c.}$ The operators $f_{\alpha is}^\dagger(t)$ and $f_{\alpha is}(t)$ are the reservoir operators defined by

$$f_{\alpha is}^\dagger(t) \equiv e^{iH_\alpha t} \left(\sum_{k \in \alpha} V_{\alpha kis}^* C_{\alpha ks}^\dagger \right) e^{-iH_\alpha t} \quad (\text{A23})$$

and

$$f_{\alpha is}(t) \equiv e^{iH_\alpha t} \left(\sum_{k \in \alpha} V_{\alpha kis} C_{\alpha ks} \right) e^{-iH_\alpha t}. \quad (\text{A24})$$

The influence functional can be evaluated using the Wick theorem and the second-order cumulant expansion method, because all the other higher order cumulants are zero at the thermodynamic Gaussian average for noninteraction leads. As a result, the ensemble average of the second-order cumulants is connected to the reservoir correlation functions $C_{\alpha ijs}^\pm(t)$, defined as

$$C_{\alpha ijs}^+(t) = \langle f_{\alpha is}^\dagger(t) f_{\alpha js}(0) \rangle_{\text{res}} \quad (\text{A25})$$

and

$$C_{\alpha ijs}^-(t) = \langle f_{\alpha is}(t) f_{\alpha js}^\dagger(0) \rangle_{\text{res}}, \quad (\text{A26})$$

where $\langle \cdot \rangle_{\text{res}}$ stands for the ensemble average of the reservoirs, and the time translation invariance is used. All LCFs in a form different from that in Eq. (A25) and Eq. (A26) are zero because the lead operators $f_{\alpha is}^\dagger(t)$ and $f_{\alpha is}(t)$ satisfy Gaussian statistics. The reservoir spectral density function is defined as

$$J_{\alpha ijs}(\omega) \equiv \frac{1}{2\pi} \int_{-\infty}^{\infty} dt e^{i\omega t} \langle \{ f_{\alpha is}(t), f_{\alpha js}^\dagger(0) \} \rangle. \quad (\text{A27})$$

with the simplified notation $\sigma = +, -$ and $\bar{\sigma} = -\sigma$, the reservoir correlation functions are associated with the spectral density functions via the fluctuation-dissipation theorem

$$C_{\alpha ijs}^\sigma(t) = \int_{-\infty}^{\infty} d\omega e^{i\omega t} f_\alpha^\sigma(\omega) J_{\alpha ijs}^\sigma(\omega), \quad (\text{A28})$$

where $J_{\alpha ijs}^-(\omega) = J_{\alpha ijs}(\omega)$, $J_{\alpha ijs}^+(\omega) = J_{\alpha jis}(\omega)$, and $f_\alpha^\sigma(\omega) = 1/(1 + e^{\sigma\beta_\alpha(\omega - \mu_\alpha)})$ is the Fermi-Dirac function for the electron ($\sigma = +$) or hole ($\sigma = -$) at the temperature $\beta_\alpha = 1/k_B T_\alpha$. For linear coupling with a noninteracting reservoir, the reservoir spectral density function can be evaluated as $J_{\alpha ijs}(\omega) = \sum_k V_{\alpha kis}^* V_{\alpha kjs} \delta(\omega - \epsilon_{\alpha k})$. After applying the Wick theorem and Grassmann algebra, the final expression of the

influence functional \mathcal{F} is

$$\mathcal{F}[\boldsymbol{\psi}] = \exp \left\{ - \int_{t_0}^t d\tau \mathcal{R}[\tau, \{\boldsymbol{\psi}\}] \right\}. \quad (\text{A29})$$

where $\mathcal{R}[\tau, \{\boldsymbol{\psi}\}] = \frac{i}{\hbar^2} \sum_{\alpha is} \mathcal{A}_{is}^\sigma[\boldsymbol{\psi}(t)] \mathcal{B}_{\alpha is}^\sigma[t, \boldsymbol{\psi}]$. Here \mathcal{A}_{is}^σ and $\mathcal{B}_{\alpha is}^\sigma$ are the Grassmann variables defined as

$$\mathcal{A}_{is}^\sigma[\boldsymbol{\psi}(t)] = d_{is}^\sigma[\boldsymbol{\psi}(t)] + d_{is}^\sigma[\boldsymbol{\psi}'(t)] \quad (\text{A30})$$

and

$$\mathcal{B}_{\alpha is}^\sigma[t, \boldsymbol{\psi}] = -i[B_{\alpha is}^\sigma(t, \boldsymbol{\psi}) - B_{\alpha is}^{\prime\sigma}(t, \boldsymbol{\psi}')], \quad (\text{A31})$$

with

$$B_{\alpha is}^\sigma(t, \boldsymbol{\psi}) = \sum_j \int_0^t d\tau C_{\alpha ijs}^\sigma(t - \tau) d_{js}^\sigma[\boldsymbol{\psi}(\tau)] \quad (\text{A32})$$

and

$$B_{\alpha is}^{\prime\sigma}(t, \boldsymbol{\psi}') = \sum_j \int_0^t d\tau C_{\alpha ijs}^{\bar{\sigma}*}(t - \tau) d_{js}^\sigma[\boldsymbol{\psi}'(\tau)]. \quad (\text{A33})$$

The LCFs play the role of memory kernels that can be expanded by a series of exponential functions with the implementation of the fluctuation-dissipation theorem together with the Cauchy residue theorem and the Padé spectrum decomposition scheme of the Fermi function

$$C_{\alpha ijs}^\sigma(t) = \sum_{m=1}^M \eta_{\alpha ijsm}^\sigma e^{-\gamma_{\alpha ijsm}^\sigma t}. \quad (\text{A34})$$

The influence of the bath enters the equations of motion with M exponentiations. The auxiliary density operators $\{\rho_j^{(n)} = \rho_{j_1 \dots j_n}\}$ are determined by the time derivative of the influence functional. The final form can be reduced to the following compact form:

$$\begin{aligned} \dot{\rho}_{j_1 \dots j_n}^{(n)} = & - \left(i\mathcal{L} + \sum_{r=1}^n \gamma_{j_r} \right) \rho_{j_1 \dots j_n}^{(n)} - i \sum_j \mathcal{A}_{\bar{j}} \rho_{j_1 \dots j_n}^{(n+1)} \\ & - i \sum_{r=1}^n (-)^{n-r} C_{j_r} \rho_{j_1 \dots j_{r-1} j_{r+1} \dots j_n}^{(n-1)}, \end{aligned} \quad (\text{A35})$$

where the index $j \equiv (\sigma sn)$ corresponds to the transfer of an electron to or from ($\sigma = +/-$) the impurity state; and the Grassmannian superoperators $\mathcal{A}_{\bar{j}} \equiv \mathcal{A}_{is}^\sigma$ and $C_j \equiv C_{ijsm}^\sigma$ are defined via their fermionic actions on an operator \hat{O} as $\mathcal{A}_{\bar{j}} \hat{O} \equiv [\hat{d}_{is}^\sigma, \hat{O}]$ and $C_j \hat{O} \equiv \eta_j \hat{d}_{is}^\sigma \hat{O} + \eta_j^* \hat{O} \hat{d}_{is}^\sigma$, respectively. The on-dot electron interactions are contained in the Liouvillian of impurities, $\mathcal{L} \equiv [H_{\text{dot}}, \cdot]$. Here $\rho_0(t) = \rho(t) = \text{tr}_{\text{res}} \rho_{\text{total}}(t)$ is the reduced density matrix, and $\{\rho_{j_1 \dots j_n}^{(n)}; n = 1, \dots, L\}$ are auxiliary density matrices, with L denoting the truncation level. The transient current through the electrode α is

$$I_\alpha(t) = i \sum_{\mu s} \text{tr}_{\text{sys}} [\rho_{\alpha \mu s}^\dagger(t) \hat{d}_{us} - \hat{d}_{\mu s}^\dagger \rho_{\alpha \mu s}^-(t)], \quad (\text{A36})$$

where $\rho_{\alpha \mu s}^\dagger = (\rho_{\alpha \mu s}^-)^\dagger$ is the first-tier auxiliary density operator obtained by solving Eq. (A35). The influence of the α reservoir can be characterized completely by the hybridization function $J_{\alpha uvs}(\omega) \equiv \pi \sum_{ks} t_{\alpha kus} t_{\alpha kvs}^* \delta(\omega - \epsilon_{\alpha ks})$. The function

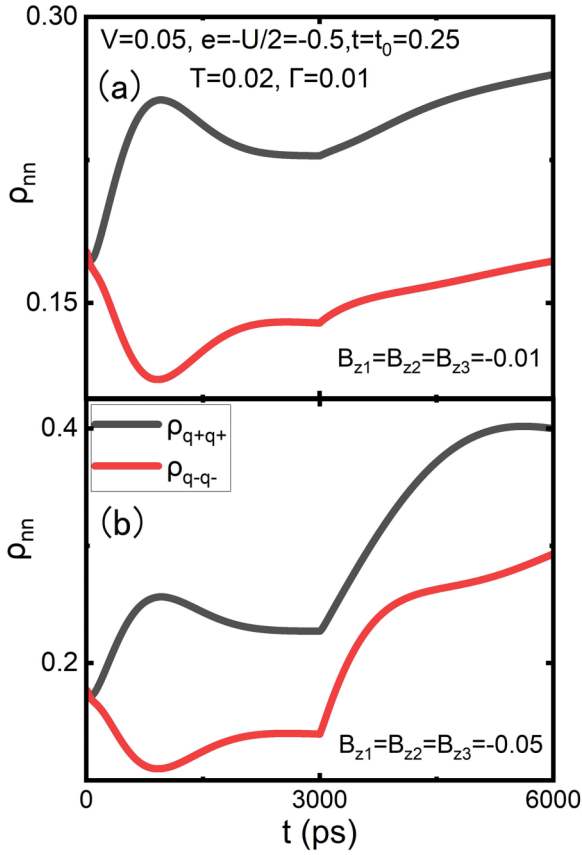


FIG. 7. When a uniform Zeeman field $B_{z1} = B_{z2} = B_{z3}$ and $\Delta B_z = 0$ is added to the TTQD system after initialization, the occupancy probability of the two chiral qubit states will evolve with time t . $B_{z1} = B_{z2} = B_{z3} = -0.01$ meV (a) and $B_{z1} = B_{z2} = B_{z3} = -0.05$ meV (b). Other structural parameters are consistent with those above.

is assumed to have a Lorentzian form here. In other words,

$$J_{\alpha uvs}(\omega) = \delta_{uv} \delta_{u1} \frac{\Delta_\alpha W^2}{(\omega - \mu_\alpha)^2 + W^2} \quad (\text{A37})$$

with bandwidth W and chemical potential μ_α . Moreover, the spectral density function for the i th QD with μ -spin can be

written as

$$A_{i\mu}(\omega) = \frac{1}{\pi} \text{Re} \left\{ \int_0^\infty dt \{ C_{a_{i\mu} a_{i\mu}^\dagger}(t) + [C_{a_{i\mu} a_{i\mu}^\dagger}(t)]^* \} e^{-i\omega t} \right\}, \quad (\text{A38})$$

and $A(\omega) = \sum_{i\mu} A_{i\mu}(\omega)$.

The HEOM approach has many advantages, such as a general form of the system Hamiltonian, which is applicable to a wide range of system parameters without additional derivation and programming efforts. The HEOM approach is nonperturbative, which can be used to treat quantum impurity systems from the perspective of open dissipative dynamics. In principle, the HEOM formalism is formally accurate for non-interacting electron reservoirs. It has the ability to achieve the same level of accuracy as the numerical renormalization group and quantum Monte Carlo approaches [54].

4. Adding uniform Zeeman field to TTQDs

In this part, we discuss the influence of the chiral qubit manipulation over time when a uniform Zeeman field is added, setting as $B_{z1} = B_{z2} = B_{z3}$ and $\Delta B_z = 0$. According to formulas (12) and (13), Rabi oscillation will disappear when a uniform Zeeman field is added to the system, with $A_{q_+ \rightarrow q_+}(t) = 0$ and $\omega = 0$.

In order to verify the correspondence between the theoretical formula and the HEOM calculation in the uniform Zeeman field, we use the HEOM equation to simulate the evolution of the two chiral qubit states after the initialization with two different uniform Zeeman fields $B_{z1} = B_{z2} = B_{z3} = -0.01$ meV and $B_{z1} = B_{z2} = B_{z3} = -0.05$ meV, which is shown in Figs. 7(a) and 7(b). In the initialization process, the system can still split into two stable chiral states due to the existence of chiral terms $\hat{S}_1 \cdot (\hat{S}_2 \times \hat{S}_3)$. However, in the process of external uniform magnetic field $\Delta B_z = 0$ regulation, the Rabi cycle disappears because the uniform magnetic field cannot make the chiral qubit state oscillate. However, with the increase of the external uniform Zeeman field, the occupancy probability of the two chiral states will increase more significantly. This is related to the fact that the large external field energy destroys the degeneracy of the spin subspace, and thus the energy level transition occurs in the spin space $S_z = 1/2$ and $S_z = -1/2$ [18,31,52]. The theoretical formulas and simulation results are perfectly fitted and corresponded.

[1] M. Russ and G. Burkard, *J. Phys.: Condens. Matter* **29**, 393001 (2017).
 [2] M. Russ and G. Burkard, *Phys. Rev. B* **91**, 235411 (2015).
 [3] C. Jones, M. A. Fogarty, A. Morello, M. F. Gyure, A. S. Dzurak, and T. D. Ladd, *Phys. Rev. X* **8**, 021058 (2018).
 [4] D. A. Vajner, L. Rickert, T. Gao, K. Kaymazlar, and T. Heindel, *Adv. Quantum Technol.* **5**, 2100116 (2022).
 [5] E. Biolatti, I. D'Amico, P. Zanardi, and F. Rossi, *Phys. Rev. B* **65**, 075306 (2002).
 [6] C. Zhang, X.-C. Yang, and X. Wang, *Phys. Rev. A* **97**, 042326 (2018).
 [7] E. A. Laird, J. M. Taylor, D. P. DiVincenzo, C. M. Marcus, M. P. Hanson, and A. C. Gossard, *Phys. Rev. B* **82**, 075403 (2010).

[8] T. D. Ladd, *Phys. Rev. B* **86**, 125408 (2012).
 [9] K. Wang, H.-O. Li, M. Xiao, G. Cao, and G.-P. Guo, *Chin. Phys. B* **27**, 090308 (2018).
 [10] D. Solenov, S. E. Economou, and T. L. Reinecke, *Phys. Rev. B* **87**, 035308 (2013).
 [11] A. Saraiva, W. H. Lim, C. H. Yang, C. C. Escott, A. Laucht, and A. S. Dzurak, *Adv. Funct. Mater.* **32**, 2105488 (2022).
 [12] P. J. Leek, J. Fink, A. Blais, R. Bianchetti, M. Goppl, J. M. Gambetta, D. I. Schuster, L. Frunzio, R. J. Schoelkopf, and A. Wallraff, *Science* **318**, 1889 (2007).
 [13] G. Burkard, T. D. Ladd, A. Pan, J. M. Nichol, and J. R. Petta, *Rev. Mod. Phys.* **95**, 025003 (2023).

- [14] D. Loss and D. P. DiVincenzo, *Phys. Rev. A* **57**, 120 (1998).
- [15] V. Lindberg and B. Hellsing, *J. Phys.: Condens. Matter* **17**, S1075 (2005).
- [16] J. Medford, J. Beil, J. M. Taylor, E. I. Rashba, H. Lu, A. C. Gossard, and C. M. Marcus, *Phys. Rev. Lett.* **111**, 050501 (2013).
- [17] S. Foletti, H. Bluhm, D. Mahalu, V. Umansky, and A. Yacoby, *Nat. Phys.* **5**, 903 (2009).
- [18] J. Xia, X. Zhang, X. Liu, Y. Zhou, and M. Ezawa, *Phys. Rev. Lett.* **130**, 106701 (2023).
- [19] D. R. Ward, D. Kim, D. E. Savage, M. G. Lagally, R. H. Foote, M. Friesen, S. N. Coppersmith, and M. A. Eriksson, *npj Quantum Inf.* **2**, 16032 (2016).
- [20] S. J. Mehl, Ph.D. thesis, Technische Hochschule, Aachen, 2014.
- [21] B. R. Buřka, T. Kostyrko, and J. Łuczak, *Phys. Rev. B* **83**, 035301 (2011).
- [22] J. Fei, Ph.D. thesis, University of Wisconsin–Madison, 2014.
- [23] K. Wang, G. Xu, F. Gao, H. Liu, R.-L. Ma, X. Zhang, Z. Wang, G. Cao, T. Wang, J.-J. Zhang *et al.*, *Nat. Commun.* **13**, 206 (2022).
- [24] M. Kjaergaard, M. E. Schwartz, J. Braumüller, P. Krantz, J. I.-J. Wang, S. Gustavsson, and W. D. Oliver, *Annu. Rev. Condens. Matter Phys.* **11**, 369 (2020).
- [25] M. Veldhorst, J. Hwang, C. Yang, A. Leenstra, B. de Ronde, J. Dehollain, J. Muhonen, F. Hudson, K. M. Itoh, A. Morello *et al.*, *Nat. Nanotechnol.* **9**, 981 (2014).
- [26] V. W. Scarola, K. Park, and S. D. Sarma, *Phys. Rev. Lett.* **93**, 120503 (2004).
- [27] J. Łuczak and B. R. Buřka, *Phys. Rev. B* **90**, 165427 (2014).
- [28] G. X. Chan and X. Wang, *Adv. Quantum Technol.* **2**, 1900072 (2019).
- [29] M. Tadokoro, R. Mizokuchi, and T. Kodera, *Jpn. J. Appl. Phys.* **59**, SGGI01 (2020).
- [30] C.-Y. Hsieh, A. Rene, and P. Hawrylak, *Phys. Rev. B* **86**, 115312 (2012).
- [31] J. Łuczak and B. R. Buřka, *Quant. Info. Proc.* **16**, 1 (2017).
- [32] C.-Y. Hsieh and P. Hawrylak, *Phys. Rev. B* **82**, 205311 (2010).
- [33] Y. Wang, Z. Zhu, J. Wei, and Y. Yan, *EPL (Europhys. Lett.)* **130**, 17003 (2020).
- [34] Y.-M. Liu, Y.-D. Wang, and J.-H. Wei, *Chin. Phys. B* **31**, 057201 (2022).
- [35] G. Tataru, H. Kohno, and J. Shibata, *Phys. Rep.* **468**, 213 (2008).
- [36] Y. Qi, Y.-M. Liu, Y.-D. Wang, J.-H. Wei, and Z.-G. Zhu, *Chin. Phys. B* **32**, 087304 (2023).
- [37] J. Hu, M. Luo, F. Jiang, R. X. Xu, and Y. J. Yan, *J. Chem. Phys.* **134**, 244106 (2011).
- [38] C.-Y. Lai, M. Di Ventra, M. Scheibner, and C.-C. Chien, *EPL (Europhys. Lett.)* **123**, 47002 (2018).
- [39] Y. Liu, Y. Chen, and Z. Wang, *Solid State Commun.* **150**, 1136 (2010).
- [40] Z. H. Li, Y. X. Cheng, J. H. Wei, X. Zheng, and Y. J. Yan, *Phys. Rev. B* **98**, 115133 (2018).
- [41] Z. H. Li, N. H. Tong, X. Zheng, D. Hou, J. H. Wei, J. Hu, and Y. J. Yan, *Phys. Rev. Lett.* **109**, 266403 (2012).
- [42] D. Hou, R. Wang, X. Zheng, N. H. Tong, J. H. Wei, and Y. J. Yan, *Phys. Rev. B* **90**, 045141 (2014).
- [43] A. H. MacDonald, S. M. Girvin, and D. Yoshioka, *Phys. Rev. B* **37**, 9753 (1988).
- [44] Y. X. Cheng, Y. D. Wang, J. H. Wei, Z. G. Zhu, and Y. J. Yan, *Phys. Rev. B* **95**, 155417 (2017).
- [45] P. A. Lee, *Handbook of High-Temperature Superconductivity* (Springer, 2007), pp. 527–568.
- [46] R. P. Feynman and F. L. Vernon Jr., *Ann. Phys.* **281**, 547 (2000).
- [47] J. Jin, X. Zheng, and Y. Yan, *J. Chem. Phys.* **128**, 234703 (2008).
- [48] L. Z. Ye, X. Wang, D. Hou, R.-X. Xu, X. Zheng, and Y. Yan, *Wiley Interdisc. Rev. Comput. Mol. Sci.* **133**, 101106 (2011).
- [49] V. W. Scarola and S. Das Sarma, *Phys. Rev. A* **71**, 032340 (2005).
- [50] Y. D. Wang, J. H. Ni, and J. H. Wei, *Phys. Rev. B* **96**, 245426 (2017).
- [51] R. Hartle and A. J. Millis, *Phys. Rev. B* **90**, 245426 (2014).
- [52] I. Weymann, B. R. Buřka, and J. Barnaś, *Phys. Rev. B* **83**, 195302 (2011).
- [53] S. K. Kehrein and A. Mielke, *Ann. Phys.* **252**, 1 (1996).
- [54] F. B. Anders, E. Lebanon, and A. Schiller, *Phys. Rev. B* **70**, 201306 (2004).
- [55] Y. X. Cheng, W. J. Hou, Y. D. Wang, Z. H. Li, J. H. Wei, and Y. J. Yan, *New J. Phys.* **17**, 033009 (2015).